

Self-assembly of Pluronic F127-diacrylate in ethylammonium nitrate: structure, rheology and ionic conductivity before and after photo-crosslinking

Carlos R. López-Barrón^{1,*}, Ru Chen², Norman J. Wagner², Peter J. Beltramo^{2,3}

¹ExxonMobil Chemical Company, Baytown Technology and Engineering Complex, Baytown, Texas 77520, United States

²Center for Neutron Science, Department of Chemical and Biomolecular Engineering, University of Delaware, Newark, Delaware 19716, United States

³Department of Materials, ETH Zürich, Vladimir-Prelog-Weg 5, 8093 Zürich, Switzerland

*corresponding author: carlos.r.lopez-barron@exxonmobil.com

Abstract

The self-assembly of an end-functionalized PEO₁₀₆-PPO₇₀-PEO₁₀₆ triblock copolymer (BCP) with acrylic end groups (Pluronic F127-diacrylate or FDA) in a protic ionic liquid (deuterated ethylammonium nitrate, dEAN), is studied using small-angle neutron scattering, shear rheology and dielectric spectroscopy. This functionalization constitutes less than 1 wt% of the copolymer and has no effect on micelle formation in dEAN. The sol-gel transition and the supramolecular crystal structure of the concentrated FDA/dEAN solutions are also found to be unaffected by the acrylation of the end groups. Photo-crosslinking results in viscoelasticity enhancement of the FDA/dEAN solutions with FDA contents below the gel point. Crosslinking gels produces soft elastomers with exceptional elasticity and conductivity comparable to the uncrosslinked solutions. Tuning BCP microstructure via self-assembly in ionic liquids followed by chemical crosslinking is shown to be a promising route for the design of materials with specific mechanical properties and ionic conductivities.

INTRODUCTION

Due their unique physicochemical properties, ionic liquids (IL) have generated both scientific interest concerning their exceptional properties, and technological interest for use conditions where these properties are of value.¹ These properties include negligible vapor pressure, high electrical conductivities (up to 100 mS/cm) with wide electrochemical windows (up to 5.8 V), as well as high electrochemical and thermal stability.^{2,3} This remarkable combination of properties make ILs very effective electrolytes^{4,5} for a number of electrochemical devices, including lithium ion batteries,⁶ solar cells,^{7,8} electromechanical actuators^{9,10} and electrolyte-gated transistors.^{11,12} Some of these application require immobilization of the IL within a quasi-solid structure, in such a way that ion transport is not compromised. This has been achieved via physical or chemical crosslinking in IL/polymer systems, both leading to the formation of solid electrolytes, also termed "ion gels".¹³

Block copolymers (BCP) are particularly versatile candidates to provide mechanical integrity via physical cross-linking because the microstructure and properties can be tuned through variations in block architecture and chemistry. BCP self-assembly is driven by solvation energy¹⁴⁻¹⁶ or other thermodynamic interactions between the IL and the BCP components.¹⁷⁻¹⁹ In particular, ion gels prepared with ABA triblock copolymers have been extensively studied.¹³⁻²¹ On the other hand, the use of chemical cross-linking to prepare ion gels has been less explored. Susan et al. reported the first chemically crosslinked ion gel containing poly (methyl methacrylate) prepared by the in situ polymerization of methyl methacrylate (MMA) in IL.²² Chemically crosslinked ion gels are usually prepared via polymerization of vinyl monomers in the presence of a crosslinking agents²²⁻²⁴ or via poly-addition reaction of macromonomers having multifunctional reactive groups²⁵⁻²⁸.

A third method to produce ion gels with enhanced mechanical properties is to combine the self-assembly provided by BCPs with subsequent chemical crosslinking steps.²⁹⁻³¹ A benefit of this approach is that the conductivity can be tuned for a specific application by design of the self-assembled microstructure, while the final crosslinked product is a solid electrolyte that can sustain mechanical loads without significant

plastic deformation. Gu and coworkers reported the synthesis of the ABA triblock copolymer poly(styrene-*b*-ethylene oxide-*b*-styrene) in which 25% of the styrene units have a pendant azide functionality²⁹. They prepared ion gels by self-assembly of this copolymer in the aprotic ionic liquid 1-ethyl-3-methylimidazolium bis-(trifluoromethyl) sulfonyl amide, followed by chemical crosslinking of the azide groups by thermal annealing. The latter step provides enhanced mechanical toughness to the ion gel without significant detriment on its ionic conductivity. Similarly, Miranda and coworkers prepared poly(propylene oxide-*b*-ethylene oxide-*b*-propylene oxide) BCPs with cross-linkable end groups³⁰. By self-assembly in the aprotic ionic liquid 1-butyl-3-methylimidazolium hexafluorophosphate and subsequent photo-crosslinking, they produced highly conductive, solid, elastic gels. Crosslinking of these polymers through their end-groups was sufficient to impart mechanical stability to the gels, which did not have a significant effect on the conductivity or the microstructure of the gels.

In this work we use an established synthetic route³² to prepare Pluronic F127-diacrylate (FDA) from commercial Pluronic F127. The latter is a poly(ethylene oxide-*b*-propylene oxide-*b*-ethylene oxide) (PEO-PPO-PEO) triblock copolymer with ~70 wt% PEO. The self-assembly and rheological response of FDA in the protic ionic liquid ethylammonium nitrate (EAN) are studied and compared to those corresponding to the non-functionalized F127/EAN system. As recently reported, F127 self-assembles into spherical micelles in EAN that further assemble into a face-centered cubic (FCC) supramolecular crystal upon increasing concentration or temperature.¹⁶ The transition from disordered to crystalline (ordered) structure manifests as a sol-gel rheological transition. Here, we show that the micellar structure as well as the sol-gel transition is virtually unaffected by the presence of the acrylate end groups. Photo-crosslinking this microstructure leads to a conductive elastomer with notable mechanical properties and conductivity, which can be varied with composition. Our results provide a platform for the design of materials with enhanced viscoelasticity or with elastomeric properties to be used in electrolyte applications. The main advantage of the synthetic strategies proposed here is the use of inexpensive, commercially available copolymers along with the ease in all the synthetic steps.

EXPERIMENTAL SECTION

Materials. Pluronic F127 (PEO₁₀₆PPO₇₀-PEO₁₀₆), dichloromethane, diethyl ether, triethylamine and acryloyl chloride were purchased from Sigma-Aldrich and used as received. Partially deuterated EAN (dEAN) was prepared by heating equimolar mixtures of ethylammonium nitrate (purchased from Iolitec) and D₂O to 40 °C for 3 h. The solution was then dried by heating to 90 °C under vacuum for 24 h and subsequently remixed with D₂O. The process was repeated three times, resulting in about 2.5 of the amino hydrogens being replaced with deuterium, as ascertained by ¹H NMR.¹⁶ The water content, measured by Karl Fischer titration after drying, was 0.13 wt %.

Synthesis of Pluronic F127 Diacrylate (FDA). FDA was synthesized following the procedure reported by Cellesi et al. In short, 50 g of Pluronic F127 was dissolved in toluene by slow stirring at room temperature under nitrogen atmosphere. The mixture was cooled down to 0 °C using an ice bath. Acrylation of the hydroxyl groups of F127 was achieved by sequential addition of 2.4 ml of trimethylamine, 40 ml of dichloromethane and 1 ml of acryloyl chloride dissolved in 40 ml of dichloromethane, followed by stirring for 12 h under nitrogen gas. The precipitated triethylammonium chloride was filtered away and the solvent evaporated using a rotary evaporator until a viscous oil was obtained. The latter was dissolved in dichloromethane, washed with DI water and dried over sodium sulfate. The product FDA was precipitated into excess chilled diethyl ether. The white precipitate was dried under vacuum for 1 day.

Preparation of FDA/dEAN solutions and cross-linking. FDA/dEAN solutions with compositions ranging from 5 to 24 wt % were prepared by weighing the corresponding quantities of block copolymer and dEAN in capped vials, followed by several cycles of strong mechanical mixing (using a vortex mixer) and centrifugation until obtaining clear, transparent solutions. These solutions were used for morphological and rheological characterization. Another set of solutions were prepared with dEAN containing the photoinitiator 1-hydroxycyclohexyl phenyl ketone with a composition of 1 wt% (w.r.t. the polymer weight). These solutions were crosslinked by exposing them to an ultraviolet (UV) light source (365nm, 9.6

mW/cm²) for 30 min, using the photo-curing accessory for the ARES-G2 rheometer (TA Instruments). A Peltier system was used to control the temperature and a 20 mm parallel plate geometry with the upper plate made of quartz was used for UV crosslinking of the sample. The sample thickness was 1 mm. The crosslinking reaction was monitored by measuring the dynamic moduli.

Rheology. Rheological characterization was performed using a stress-controlled rheometer (DHR-3, TA Instruments) using parallel plates of diameter = 40 mm. Dynamic temperature ramps were performed using angular frequency $\omega = 1$ rad/s and strain amplitude $\gamma_0 = 5\%$. Dynamic frequency sweeps were carried out at different temperatures ranging from 15 °C to 40 °C with $\gamma_0 = 5\%$. Dynamic time sweeps were performed during photo-curing in the ARES-G2 rheometer with 20 mm parallel plate geometry with $\omega = 10$ rad/s and $\gamma_0 = 1\%$. The samples were loaded at 15 °C, and equilibrated at the measurement temperature (15, 25 or 40 °C) for 10 min. Subsequently, the dynamic moduli was measure for 60 s before the UV light was turned on, and for 10 min during the photo-curing reaction.

Tensile tests. Tensile tests measurements were performed using a Sentmanat extensional rheometer (SER)³³ mounted on a stress-controlled rheometer MCR 501 (Anton Paar). Strips of crosslinked FDA/dEAN solutions (with 24 wt% FDA) are attached to the drums of the SER using double-sided masking tape (3M 410MTM). To completely avoid slip on the drums a UV-curing adhesive (Loctite 352TM) is applied to cover both the sample strip and the tape, and subsequently cured with a UV lamp. After curing, the adhesive forms a though bond between the sample and the tape that remains intact after tensile test. The strips were uniaxially stretched at room temperature, using a constant Hencky strain rate 0.01 s⁻¹.

Small-Angle Neutron Scattering (SANS). FDA/dEAN solutions with and without photoinitiator were loaded in titanium cells with 1 mm path length, using quartz windows. The samples containing photoinitiator were crosslinked inside the cells by exposing them to the UV light source through the cell windows for 30 min. SANS measurements were performed at the NIST Center for Neutron Research (NCNR) in Gaithersburg, MD, on the NG7 30 m SANS instrument, using neutrons with wavelength $\lambda = 6$

Å, and wavelength spread $\Delta\lambda/\lambda = 0.11$. The temperature was maintained to ± 0.1 °C using a circulating bath. Three sample-to-detector distances were used (1, 4, and 13 m) to cover a q -range from 0.003 to 0.4 Å⁻¹. Raw SANS data were corrected for sample transmission, background radiation, sample thickness, and detector sensitivity using IGOR macros available from NCNR. Data were averaged azimuthally to obtain one-dimensional plots of intensity versus scattering wave vector, $I(q)$. The SANS data for the low concentrated solutions were fitted with a “spherical core-shell model”,^{34, 35} whereas a FCC lattice model with paracrystalline distortion^{36, 37} was used to fit the SANS data for the concentrated solutions. These models are presented in the Supporting Information (SI).

Conductivity measurements. Conductivity measurements were performed using a specially designed parallel plate electrode dielectric spectroscopy cell attached to an Agilent 4294A-1D5 impedance analyzer.³⁸ The measurement cell consists of a pair of stainless steel electrodes clamped around an acrylic spacer, which serves as the sample chamber. Liquid samples are carefully loaded with a syringe, avoiding the development of any air bubbles that would alter the spectra. Frequency sweeps are made from 110 MHz to 40 Hz at a nominal oscillator voltage of 0.5 V. The temperature is controlled to ± 0.5 °C by flowing silicone oil through cylindrical bores in the electrodes and measurements are taken from 20 °C to 60 °C in 5 °C increments. Open/short compensation is performed to remove stray impedances in parallel and in series with the sample. The corrected impedance spectra, $Z^*(\omega)$, is interpreted as a frequency dependent conductivity and dielectric constant as

$$\frac{1}{Z^*(\omega)} = \left[\sigma(\omega) + i \epsilon_0 \omega'(\omega) \right] \quad (1)$$

where ϵ_0 is the measured cell constant based on the spacer geometry, $\sigma(\omega)$ is the conductivity, ω is the angular frequency, ϵ_0 is the permittivity of free space and $\epsilon'(\omega)$ is the dielectric constant. For measurements of cross-linked samples, the sample was loaded into the acrylic spacer and clamped between one electrode and a glass slide to accelerate the UV curing process. After curing, the glass slide was

removed, the complete cell assembled, and measurements taken using the same protocol as the liquid samples.

RESULTS AND DISCUSSION

Micellar structure. The microstructure of (non-crosslinked) FDA/dEAN solutions was elucidated using SANS measurements. Figure 1(a) shows SANS profiles of a 5 wt% FDA/dEAN solution at 30 °C. The typical scattering profile corresponding to the form factor of spherical objects is observed. These data is well fitted with the core-shell model (solid line), described in the SI. A small intensity upturn is observed at low q -values, which could indicate mesophase formation whose origin may be solvophobic interactions between the d-EAN and the PEO block, as previously reported in PEO and Pluronic aqueous solutions.³⁹⁻⁴¹ SANS measurements at different temperatures and compositions, along with the fitting parameters to the core-shell model (Table S1), are given in the SI. From the fittings, we found that the micelle radius is ~ 7 nm and is practically independent of temperature and concentration over the ranges probed. The micelle size is practically the same for the micelles formed with F127 and with FDA (see Table S1), which indicates that the presence of the acrylate groups at the ends of the block copolymer have no effect on the micelle formation. Previous reports show that, near the critical micellar temperature (CMT), the PPO micelle core in Pluronic aqueous solution contain significant amount of water, which is replaced by polymer chains as the temperature increases.^{42, 43} As described in the SI, fitting of the SANS data for the 5 wt% FDA/dEAN solutions to a three parameter model that combines species mass balance to solve for core radius, R_c , shell (corona) thickness, T_s , and volume fraction of dEAN in the core, $\phi_{\text{dEAN-in-core}}$, provides evidence that F127 and FDA micelles formed in dEAN have nearly dry micelle cores, with $\phi_{\text{dEAN-in-core}} < 0.1$.

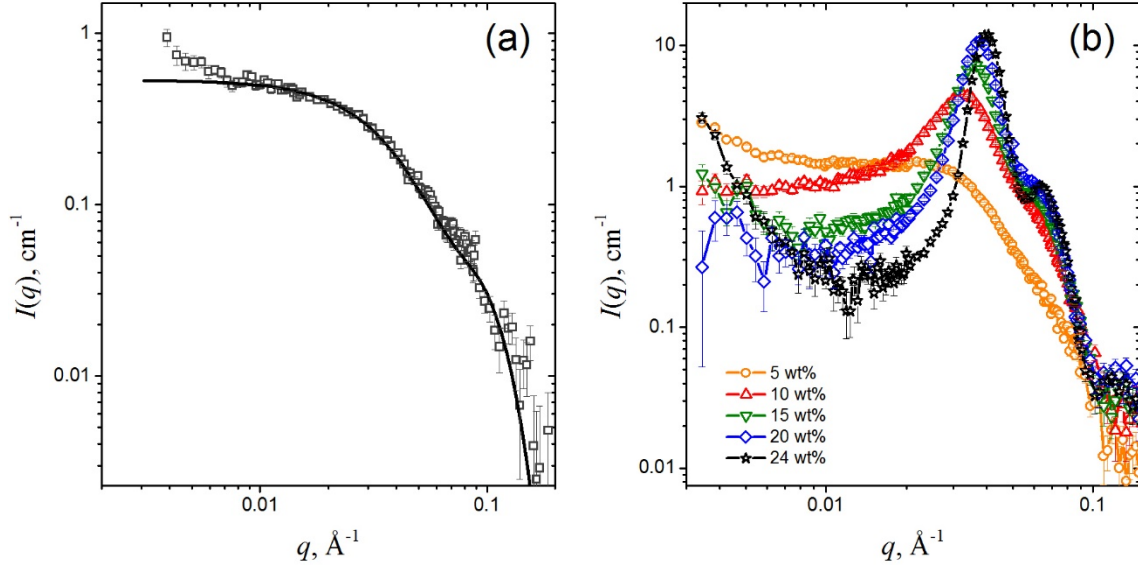


Figure 1. (a) SANS profiles of a 5 wt % FDA/dEAN solutions measured 30 °C. Solid line is best fit to the core-shell model described in the SI. (b) SANS profiles of FDA/dEAN solutions with the indicated concentrations, measured at 40 °C.

The aggregation number, N_{agg} , and the volume fraction of dEAN in the corona, $\phi_{\text{dEAN-in-corona}}$, are given in Table S1. N_{agg} increases with temperature as a consequence of the decrease in solubility due to the weakening of hydrogen bonds between the amino hydrogens (or deuteriums) in dEAN and the oxygens in the PEO blocks. This also leads to a slight decrease in $\phi_{\text{dEAN-in-corona}}$ with temperature, which reflects the dEAN desorption from the micelle corona. Further increasing the temperature to 40 °C causes the appearance of a scattering peak (see Figure S1(a)), suggesting intermicellar interaction at high temperatures. This is consistent to the recently reported behavior of non-functionalized F127/dEAN solutions.¹⁶ As expected, the intermicellar scattering peak is more pronounced at higher polymer concentrations (Figure 1(b)) and higher temperatures for compositions up to 20 wt% (see Figure S2). Additionally, the mean peak position changes with composition. As shown in Figure S3, the characteristic intermicellar distance, calculated as $d = 2 / q^*$, where q^* is the position of the main scattering peak, decreases with

composition. However, no change with temperature is observed in the solutions before and after crosslinking.

Sol-gel transition. Figure S2(c) shows that increasing the temperature in the 20 wt% sample, the main scattering peak becomes sharper and the intensity of the shoulder on this peak becomes more intense. This indicates the transition to a more ordered structure. Dynamic moduli measurements during temperature ramps were employed to further explore this transition. Figure 2(a) shows the dynamic moduli as a function of temperature for FDA/dEAN solutions with different composition. A sol-gel rheological transition upon heating is characterized by the sharp increase in five orders of magnitude in the elastic modulus. This behavior is virtually identical to that observed in the F127/dEAN system, as recently reported.¹⁶ The temperature at which the sol-gel transition occurs, T_{gel} , is plotted as a function of composition in Figure 2(b) for both F127/dEAN (adapted from López-Barrón et al.¹⁶) and FDA/dEAN solutions. Note that the gel point is not affected by the presence of the acryloyl groups in the copolymer. This is expected, as these groups represent less than 1 wt% of the copolymer. Therefore, the overall hydrogen bonding strength between the oxygens in the PEO blocks and the amine group in dEAN is virtually unchanged after the acrylation of F127.

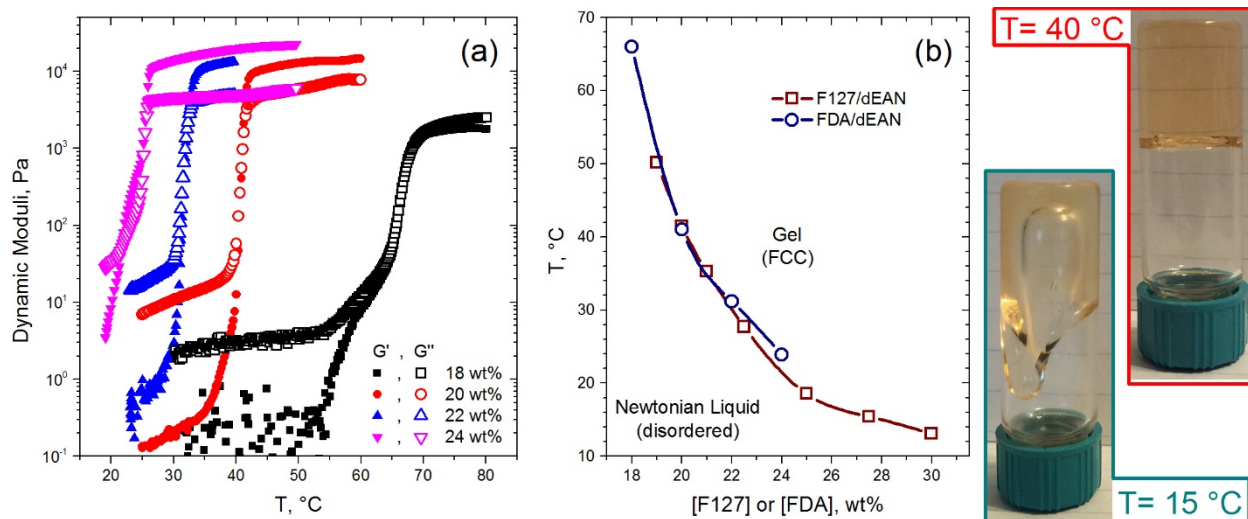


Figure 2. (a) Dynamic moduli as a function of temperature for FDA/dEAN solutions with the indicated composition. (b) Phase diagram of F127/dEAN¹⁶ and FDA/dEAN. Right panel shows pictures of glass vial containing a 24 wt % FDA/dEAN solution at the indicated temperatures.

The elastic and viscous moduli (G' and G'' , respectively) as a function of angular frequency for a 24 wt % FDA/dEAN solution are shown in Figure 3(a). As shown in Figure 2, T_{gel} for this sample is ~ 24 °C. Below that temperature, the scaling behaviors of the dynamic moduli at low frequencies are $G' \sim \omega^{-2}$ and $G'' \sim \omega^{-1}$ (Figure 3(a)), which indicates liquid-like behavior. This is confirmed by the constant value of the complex viscosity with frequency, as shown in Figure 3(b). At 25 °C, the dynamic moduli showed a sharp upturn at low frequencies, which reflects the fact that the sample was just above the gel temperature and, therefore, gelation occurred during the test (the frequency sweep was performed from high to low frequency values, as indicated by the arrows in Figure 3). At $T > 25$ °C, the sample is more elastic than viscous (i.e., $G' > G''$) and the elastic modulus is nearly independent on frequency ($G' \sim \omega^{0.2}$), at low frequencies. We were not able to measure the frequency corresponding to the modulus crossover ($\omega_{\text{crossover}}$), which could be used to calculate the characteristic relaxation time of the sample, $\tau = 1/\omega_{\text{crossover}}$. However, if the moduli cross, they will do it at a frequency lower than $\sim 5 \cdot 10^{-4}$ rad/s, hence the relaxation time is > 30 min. The plateau value of $G' > 10^4$ Pa is consistent with a cubic structure,⁴⁴ which is confirmed by SANS measurements, as discussed below. The gel behavior is also characterized by a pronounced frequency-thinning under dynamic flow that spans over at least six decades in frequency Figure 3(b).

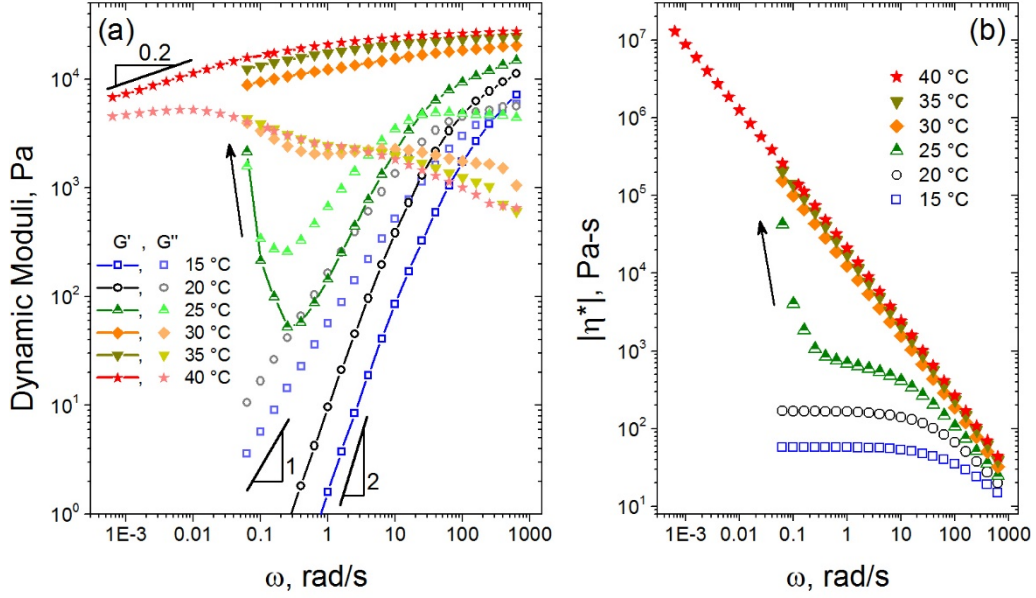


Figure 3. (a) Dynamic moduli and (b) complex viscosity versus frequency for a 24 wt % FDA/dEAN solution measured at the indicated temperatures. The arrows indicates the direction of the frequency sweep inducing in gelation.

As in F127/dEAN solutions,¹⁶ the origin of the sol-gel rheological transition in FDA/dEAN is a structural order-disorder transition (ODT). Figure 4 shows SANS profiles of the 24 wt% FDA/dEAN solution at three different temperatures. The single, broad scattering peak observed at 15 °C (below the gel transition) indicates a disordered liquid state, which explains the low viscosity observed in Figure 3(b). Above T_{gel} (~24 °C for this sample), the peak sharpens and a Bragg reflection appears, indicating the formation of a crystalline lattice. These data was fit to two crystalline models: body-centered cubic (BCC) and face-centered-cubic (FCC) lattice with paracrystalline distortion.^{36, 37} The latter model is described in the SI. Similar to the gels formed in F127/dEAN solutions,¹⁶ the data for the FDA/dEAN gels are best fitted with the FCC model. This indicates that the functionalization of F127 has negligible effect on the microstructure of the solution in dEAN. The FCC model fitting provides values of sphere radius, R , and the nearest-neighbor separation, D . These geometrical parameters are given in Table S2. The values of the lattice

parameters for the F127/dEAN and the FDA/dEAN gels are identical ($R = 5$ nm and $D = 28$ nm), which provides further evidence that the acrylation of the triblock end groups has no effect on the crystalline structure of these gels.

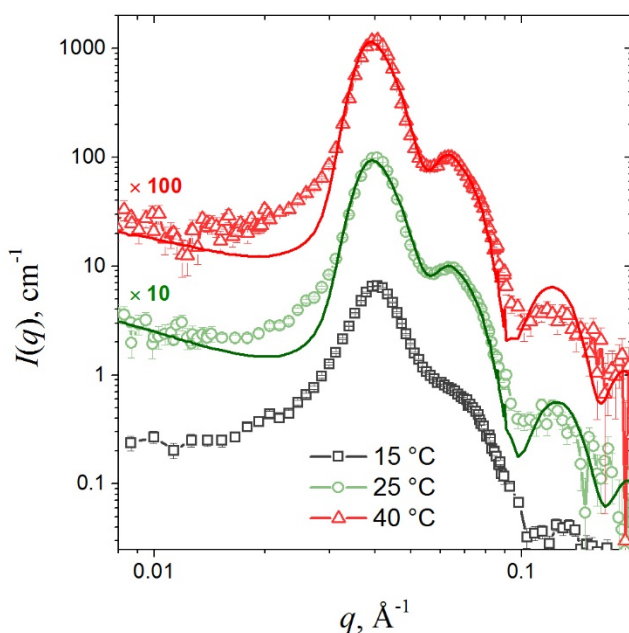


Figure 4. SANS data from a 24 wt % FDA/dEAN solution measured at the indicated temperatures. Solid lines are best fits to face-centered cubic (FCC) lattice model with paracrystalline distortion. Data at 25 °C and 40 °C are vertically shifted (by the indicated factor) for clarity.

Rheology and microstructure of crosslinked solutions. The evolution of the dynamic moduli during UV-curing at 25 °C of the FDA/dEAN solutions with compositions ranging from 5 to 20 wt% is shown in Figure 5(a). Before crosslinking, all the solutions behave as Newtonian liquids, which is evidenced by the low viscosity that is independent of the frequency (Figure 5(f)). Crosslinking the solution with 5 wt% FDA results on a slight, but measurable, increase in viscosity without altering its Newtonian character. This can be explained by the fact that at this composition micelles do not interact with each other, and therefore,

crosslinking occurs mostly within the corona of individual micelles (intra-micellar crosslinking). Hence crosslinking only produces slightly ‘harder’ micelles, but not network formation. In contrast, crosslinking the 10 wt% solution results in at least two orders of magnitude increase in moduli and viscosity. Additionally the crosslinked solution develops a viscoelastic character and the frequency-thinning (Figure 5(f)) observed in the high frequency regime.

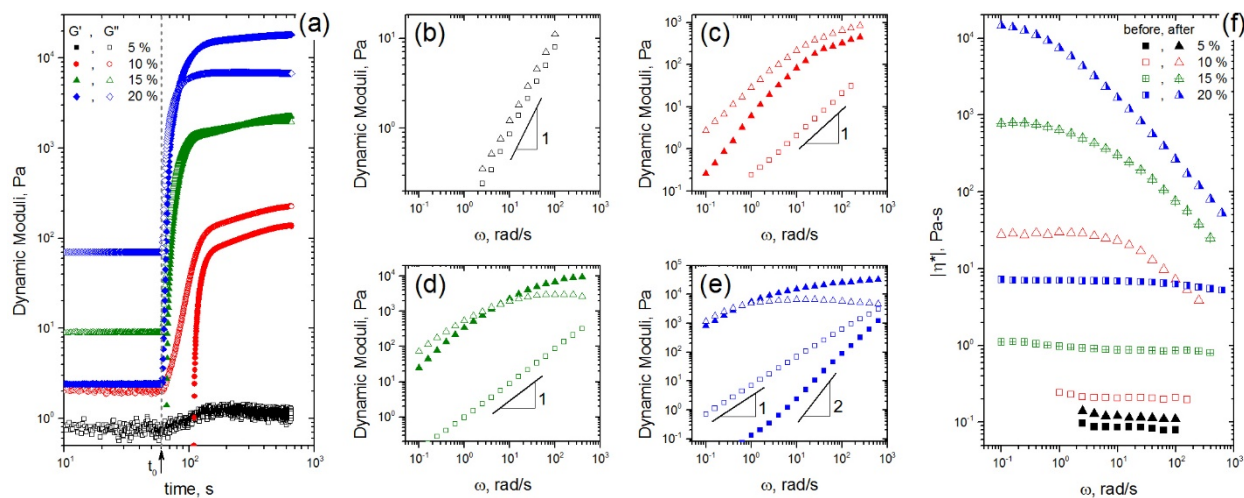


Figure 5. (a) Dynamic moduli versus time during photo-crosslinking of FDA/dEAN solutions. UV light was turned on after 60 s of starting the test, as indicated by the arrow, and denoted as t_0 . (b)-(e) Dynamic moduli as a function of frequency for FDA/dEAN solutions with (b) 5 wt%, (c) 10 wt%, (d) 15 wt% and (e) 20 wt% FDA, before (squares) and after (triangles) crosslinking. Filled and empty symbols correspond to G' and G'' , respectively. (f) Complex viscosity as a function of frequency for solution with the indicated FDA wt%. All the measurements were performed at 25 °C.

The viscosity increase upon crosslinking is more pronounced (~3 orders of magnitude) for the 15 and 20 wt% solutions. In addition, these two solutions develop a rubbery plateau modulus of 12 kPa and 40 kPa, respectively, which suggest the formation of a supramolecular structure that likely have some inter-micellar

crosslinking. This is expected, as the micelles at these concentrations exhibit pronounced scattering peaks (Figure 1(b)). The characteristic relaxation time for these crosslinked solutions, obtained from the inverse of the frequency where G' and G'' crossover, are 0.18 s and 1.5 s for the 15 wt% and 20 wt% solutions, respectively. Despite the large increase in viscoelasticity, crosslinking of these solutions does not produce an elastomer or a gel. Rather a highly elastic liquid with strong shear-thinning behavior is formed.

The morphology of the crosslinked solutions was characterized by SANS. Figure 6(a) shows the SANS profiles of a 5 w% FDA/dEAN solution crosslinked at 25 °C. The scattering of this solution measured at $T = 30$ °C can be fitted with same spherical core-shell model used to fit the data corresponding to the non-crosslinked solution (Figure 1). The fitting parameters are given in Table S1. Interestingly, the response to increasing temperature does not change after crosslinking this solution. For both solutions (non-crosslinked and crosslinked), a scattering peak appears upon heating above 40 °C. On the other hand, the intensity upturn at low q -values is more pronounced for in the crosslinked solutions, which could result from micelle clustering during crosslinking.

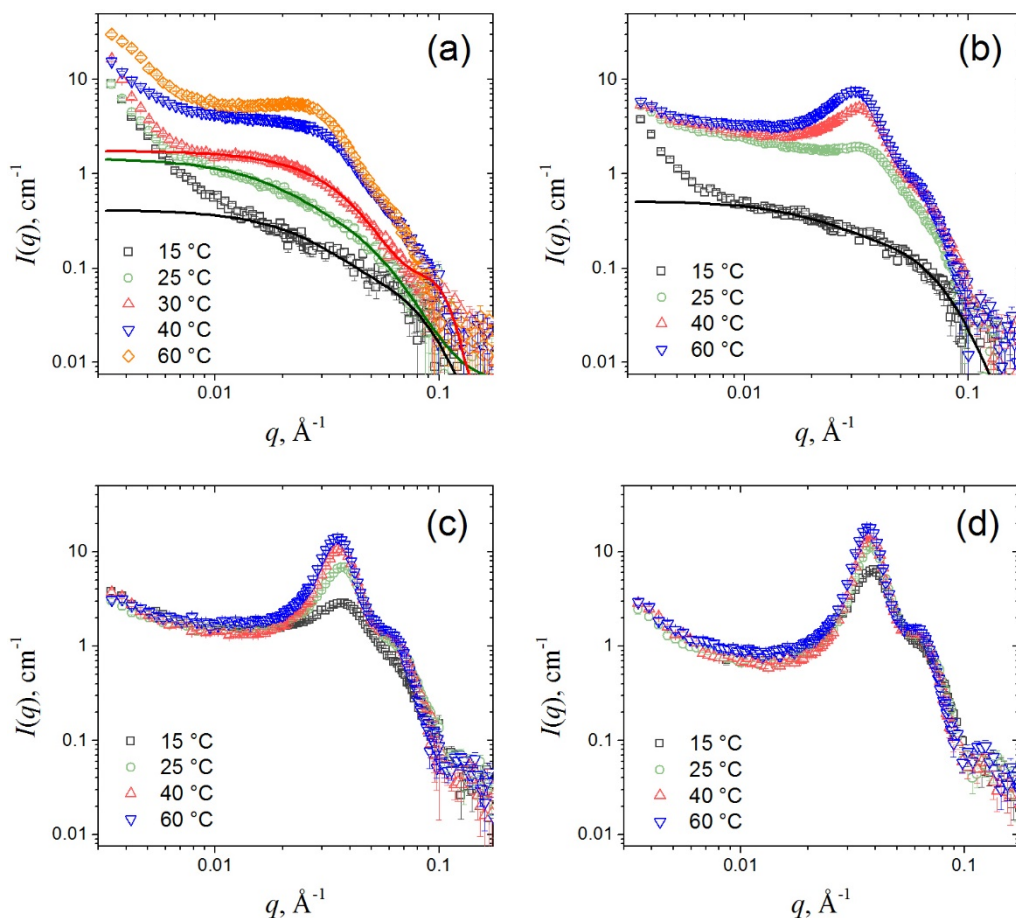


Figure 6. SANS profiles of crosslinked FDA/dEAN solutions, with (a) 5 wt%, (b) 10 wt%, (c) 15 wt% and (d) 20 wt% FDA. All four solutions were crosslinked at 25 °C, and the SANS measured were carried out at the indicated temperatures.

The SANS profiles and temperature response of the solutions with compositions from 10 to 20 wt% (Figure 6(b)-(d)) are nearly identical to the non-crosslinked solutions (see Figure S2). The strikingly similar thermal response of the solutions before and after photo-curing is explained by the low crosslinking density obtained due to the fact that each copolymer molecule only has two functional groups, i.e., only two crosslinking points. Hahn and coworkers showed that the ODT temperature, T_{ODT} , as well as the structure below and above T_{ODT} of a polystyrene-polyisoprene (PS-PI) diblock copolymer is unaffected by slightly crosslinking

the PI block.⁴⁵ The relatively low crosslinking density in their systems enables a reversible ODT, which demonstrates the existence of diffusionless phase transitions (i.e., transitions that does not require macroscopic molecular diffusion) in crosslinked block copolymers. Therefore, it is not surprising that the thermal transitions in our solutions are unaffected by crosslinking, given that only two functional groups per molecule produce a very low crosslinking density.

At concentrations close to the sol-gel line (Figure 2(b)) photo-curing induces a transition very different to that observed at low concentrations. Figure 7(a) shows the evolution of the dynamic moduli of a 24 wt% FDA/dEAN solution during the photo-curing reaction at two temperatures: 15 °C (below T_{gel}) and 40 °C (above T_{gel}). At both temperatures, the moduli reaches a plateau before 5 min of exposure to UV light. The sample crosslinked at 40 °C reaches a higher elastic modulus than that crosslinked at 15 °C. This reflects differences in microstructure. Figure 7(b) shows the dramatic transition from a Newtonian liquid to a soft solid when the solution is crosslinked at 15 °C. The soft solid behavior is characterized by the elastic modulus being nearly independent on frequency ($G' \sim \omega^{0.26}$). As discussed above, the solution at 40 °C behaves as a gel due to formation of a FCC cubic lattice. Figure 7(c) shows that photo-curing at 40 °C produces an additional, threefold increase in the elastic modulus at 40 °C, while Figure 7(d) shows that a similar modulus can be obtained by crosslinking in the liquid state at 15 °C and then heating to 40 °C. Cooling a crosslinked sample from 40 °C to 15 °C returns it to a lower modulus state. This shows that the equilibrium mechanical properties are dominated by the phase behavior.

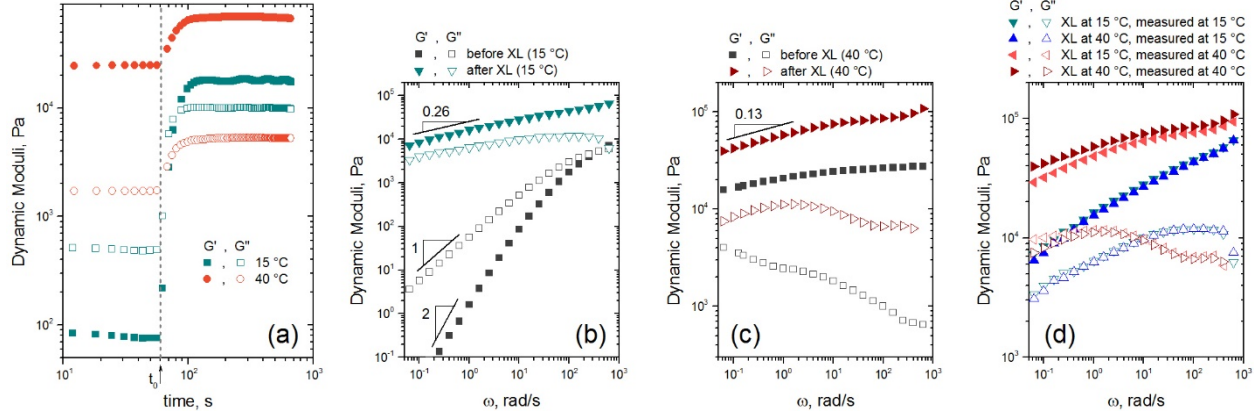


Figure 7. (a) Dynamic moduli versus time during photo-crosslinking (at 15 °C and 40 °C) of a 24 wt% FDA/dEAN solution. UV light was turned on after 60 s of starting the test, as indicated by the arrow and denoted as t_0 . (b)-(d) Dynamic moduli as a function of frequency for a 24 wt% FDA/dEAN solutions with before and after crosslinking. In (b) the solution was crosslinked and measured at 15 °C and in (c) crosslinked and measured at 40 °C.

It should be noted that crosslinking the 24 wt% solution not only enhances its mechanical strength, but produces radically different materials. These materials are better described as soft elastomers (or non-thermo-reversible gels) with remarkably high stretchability, as illustrated in Figure 8(a). Stress-strain curves of the solutions crosslinked at 15 °C and 40 °C are shown in Figure 8(b). Both samples showed similar features, namely, an initial elastic regime, followed by yield at Hencky strain (ϵ_H) ~ 0.1 , and very pronounced strain hardening with onset at $\epsilon_H \sim 0.5$. The sample crosslinked at 40 °C has slightly higher Young's modulus (54 kPa) than the one crosslinked at 15 °C (35.7 kPa). A strikingly large strain-to-break of more than 3000 % was measured in both samples. However, the measured (Hencky) strain-to-break values, measured by triplicate, show relatively high variability. These values are $\epsilon_H = 4.5 \pm 0.8$ for the sample crosslinked at 15 °C, and $\epsilon_H = 4.7 \pm 0.3$ for the one crosslinked at 40 °C. Figure 8(b) also shows that these samples can sustain remarkably high uniaxial loads before breaking. The measured tensile

strength for the samples crosslinked at 15 °C and 40 °C are 6.2 ± 1.8 MPa and 6.9 ± 0.7 MPa. Additionally, these samples show very good elastic recovery, as illustrated in the photograph taken after stretching a specimen to ~ 600 % strain Figure 8(a). The mechanism responsible for the unusual tensile properties observed in our samples is not fully understood. We hypothesize that the mechanism of the observed plastic response and super-stretchability of the crosslinked sample is a result of a complex organization of the crystalline micellar structure, as this consists of intra-micellar crosslinks at the micelle corona and inter-micellar crosslinks that can be adjacent (between corona of “adjacent” micelles) or bridged by block copolymer chains that are in solution (see Figure 8(c)). Additionally, the measured strain hardening could result from an energetically expensive process (such as disentanglements, pull-outs and bridging of polymer chains between micelles) occurring when the deformation surpasses the maximum strain allowed by the maximum chain stretching and micelle reorganization processes. These hypotheses are being investigated further using in-situ small angle scattering techniques.

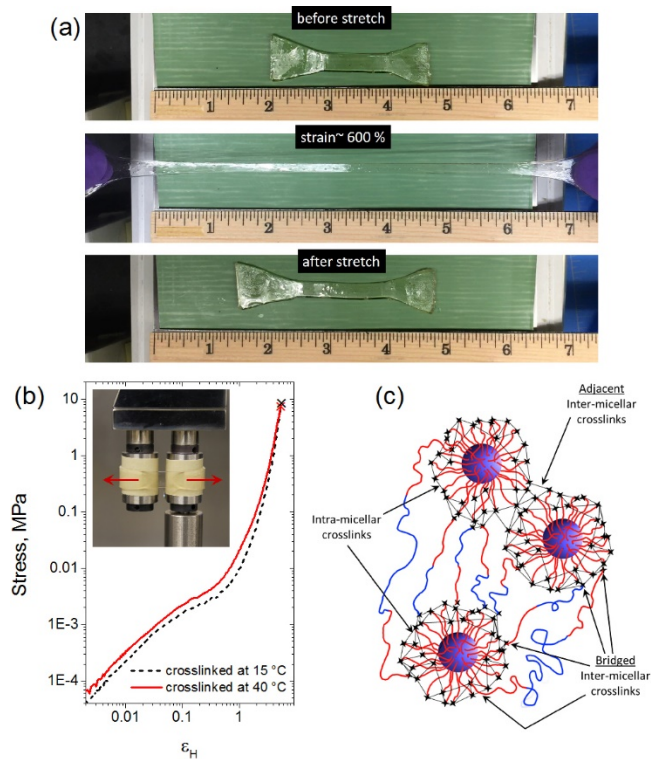


Figure 8. (a) Photographs of a strip made of crosslinked 24 wt% FDA/dEAN solution, before, during and after being stretched. (b) Stress-strain curves for 24 wt% FDA/dEAN solutions crosslinked at 15 °C and 40 °C. The samples were deformed with a constant Hencky strain rate 0.01 s^{-1} . Inset: photograph of a crosslinked film loaded on the SER. (c) Schematics of the proposed network structure of the crosslinked concentrated FDA/dEAN solutions.

An interesting question is whether the microstructure of these soft elastomers is locked during the photo-crosslinking, and how this depends on the crosslinking temperature. Hahn et al.⁴⁵ reported that, by increasing the crosslinking density of their PS-PI diblock copolymers, the structure is locked and ODT does not occur. In contrast, structural ‘locking’ does not occur in our 24 wt% FDA/dEAN solution. Figure 7 (d) shows that the shear modulus of the photo-cured samples increases with temperature, regardless of the temperature at which they were crosslinked. The dynamic moduli of the sample crosslinked at 15 °C and measured at 15 °C are indistinguishable to those of the sample crosslinked at 40 °C and measured at 15 °C. Similarly, the moduli of the sample crosslinked at 40 °C and measured at 40°C are very close to those of the sample crosslinked at 15 °C and measured at 40 °C. This indicates that, upon crosslinking, the microstructure still responds to temperature changes but in a different way than before being crosslinked. As the system loses its fluidity due to the covalent network formation, it cannot recover Newtonian fluid behavior upon cooling. That is to say, the dynamic moduli of the crosslinked sample measured at 15 °C do not show the scaling behaviors at low frequencies corresponding to terminal behavior ($G' \sim \omega^2$ and $G'' \sim \omega$), as they do for the uncrosslinked sample (see Figure 3 or Figure 7b). To understand the nature of the transition, we performed SANS measurements on the samples crosslinked at both temperatures.

Figure 9 shows SANS profiles of the samples that were crosslinked at 15 °C (Figure 9(a)) and 40 °C (Figure 9 (b)). The solid lines are best fits to the FCC lattice model. Note that a good fit was obtained to the data measured at 15 °C, which shows a narrower peak and better defined Bragg reflection than those observed in the non-crosslinked solution measured at 15 °C (Figure 4). Increasing the temperature has two effects:

(1) the main scattering peak becomes narrower brighter, and (2) the main peak position shifts slightly to lower q values. These effects are quantified in Table S2, which shows the geometrical parameters of the FCC lattice obtained by the fitting. Comparison of the parameters values identifies the following behaviors: (1) Both the micelle radius, R , and the volume fraction of the lattice, ϕ_{latt} , are practically the same before and after photo-curing and (2) R and ϕ_{latt} are independent of the crosslinking temperature, but they slightly increase with temperature once the solutions are crosslinked. In the uncrosslinked FDA/dEAN samples, the changes in R and ϕ_{latt} are explained by the increase in N_{agg} with temperature, as discussed above. One would expect that N_{agg} is essentially fixed for the crosslinked samples. Hence, the increase in R and ϕ_{latt} may be due simply to chain conformation changes induced by temperature. This hypothesis could be verified by NMR and theoretical studies.⁴⁶

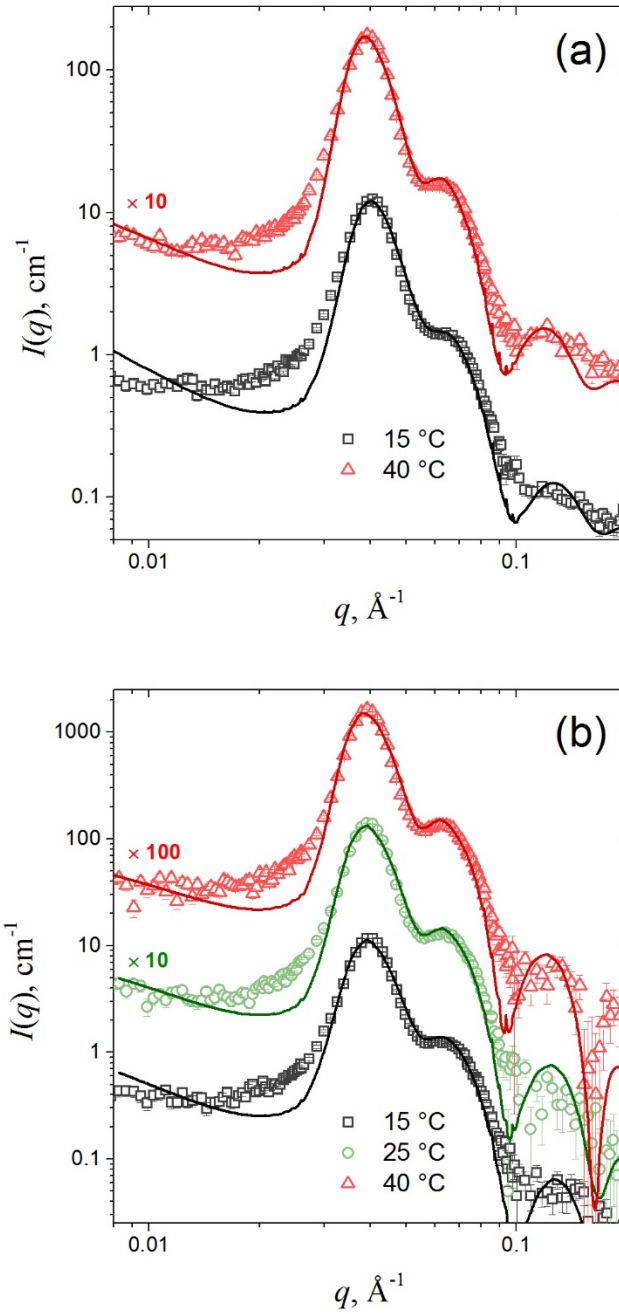


Figure 9. SANS profiles for the 24 wt% FDA/dEAN solution crosslinked (a) at 15 °C and (b) at 40 °C. SANS was measured at the indicated temperatures. Measurements at 25 °C and 40 °C are vertically shifted (by the indicated factor) for clarity.

Ionic conductivity before and after crosslinking. Figure 10(a) shows the conductivity, κ (measured at a frequency of 1 MHz), as a function of temperature for dEAN and for the 15 wt% and the 22.5 wt% FDA/dEAN solutions before and after crosslinking. Note that the frequency of 1 MHz was chosen since it is in the plateau region ($\omega > 0.1$ MHz) where electrode polarization effects are absent from the conductivity spectra for all samples (see Fig 10(b) and SI). As expected, the conductivity of the solutions is lower than that of neat dEAN. The temperature dependence of the ionic conductivity is well described with a simple Arrhenius equation $\kappa = A \exp(-E_a/RT)$, where A is a temperature independent pre-exponential factor, E_a is the activation energy, and R is the universal gas constant. The solid lines in Figure 10(a) are best first to the Arrhenius equation for dEAN and the FDA/dEAN solutions, and the inset shows the activation energies obtained by the fittings. The effect of adding FDA to the ionic liquid is a slight increase in the activation energy. This change in activation energy results in an additional subtle effect, namely, the difference between the conductivity of the solutions and neat dEAN decreases with temperature. This can be explained by the fact that ion-binding to the micelle corona in FDA/dEAN solutions occurs, hindering transport. This binding is driven by hydrogen-bonding between dEAN and the PEO blocks in FDA, which are weakened as temperature increases.^{47, 48} Therefore, increasing temperature promotes unbinding of the EAN ions from the micelles and, therefore, transport of ions is effectively increased, reducing the conductivity difference between neat dEAN and FDA/dEAN solutions. A similar conductivity dependence on temperature was observed in dEAN solutions of small ionic surfactants.^{49, 50}

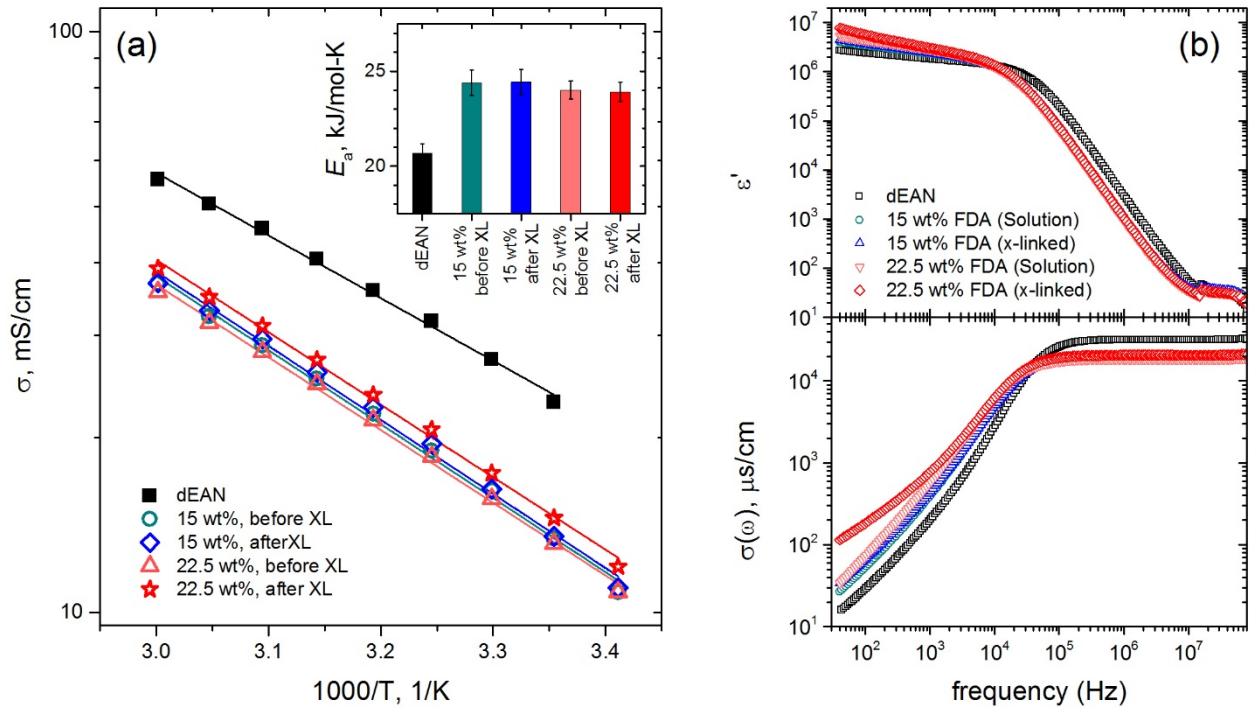


Figure 10. (a) Arrhenius plot of ionic conductivity for dEAN and FDA/dEAN solutions measured before and after crosslinking. Solid lines are best fits to Arrhenius equation. Inset: activation energy calculated by fitting data to Arrhenius equation. (b) Dielectric constant (ϵ') and the imaginary part of the conductivity ($\sigma''(\omega)$) as a function of frequency at 35 °C, at indicated compositions.

Figure 10(b) shows the frequency dependent dielectric spectra for the the 15 wt% and 22.5 wt% FDA solutions before and after cross-linking, along with than of neat dEAN. As explained in the SI, the upturn in ϵ' at low frequencies is due to electrode polarization. The addition of FDA has the effect of shifting the effects of electrode polarization to lower frequencies. We find that the shift in the electrode polarization effects in the spectra is greater than what would be expected by considering only the reduced concentration of dEAN in the 15 wt% and 22.5 wt% samples. Therefore, the addition of polymer hinders the ion motion, supporting our hypothesis of ion-binding to the micelle-corona.

Notice that the ODT for the 22.5 wt% FDA solution occurs at ~ 30 °C (see Figure 2(b)). As discussed above such transition is marked by an increase of five order of magnitude in elastic modulus. Notably, the ODT is not marked by any signal in the conductivity dependence on temperature. Indeed, κ increases monotonically from $T < T_{gel}$ to $T > T_{gel}$ with no abrupt transition observed. A similar absence of an abrupt conductivity change was recently reported for two lyotropic liquid crystal systems containing dEAN as the liquid phase.^{49, 50} One of these includes an isotropic to hexatic transition in ellipsoidal micelles made of hexadecyltrimethylammonium bromide (CTAB) and dEAN⁵⁰ and the other is an sponge to lamellar transition in didodecyldimethylammonium bromide (DDAB)/dEAN solutions.⁴⁹ Similar to the system studied here, both transitions are marked by distinct rheological sol-gel transitions. The common feature between those two systems and the one studied here is that the topology of the system remains unchanged during the sol-gel transition, i.e., no aggregation or breakage of micelles (in CTAB/dEAN and FDA/dEAN) or membrane breakage (in DDAB/dEAN) occur upon the phase transition. In this scenario, the conductivity decreases with temperature could be simply due to a decrease in ion mobility and/or to solvation of the micelle surface.

As shown in Figure 10, upon crosslinking, the conductivity increases slightly for both compositions. Miranda and coworkers³⁰ reported the opposite behavior in a series of ion gels prepared with cross-linkable PPO–PEO–PPO triblock copolymers, cross-linkable PEO homopolymers and the ionic liquid [BMI][PF6]. All their solutions show a slight decrease in conductivity upon crosslinking. Similar decrease in conductivity was reported by Gu et al.²⁹ in crosslinked ion gels made of poly(styrene-*b*-ethylene oxide-*b*-styrene) triblock copolymers in the ionic liquid [EMI][TFSA]. Importantly, our results demonstrate that the gain in mechanical reinforcement by crosslinking the FDA/dEAN solutions does not compromise their conductivity, which is consistent with previous studies.^{29, 30}

CONCLUSIONS

We report the fabrication of mechanically robust and highly conductive ion gels based on the protic IL, EAN, and an end-functionalized amphiphilic triblock copolymers (Pluronic F127-diacrylate) via UV-initiated crosslinking. This approach takes advantage of the self-assembly of the triblock copolymer in the IL, to create the desired micellar structure, and the subsequent chemical bonding to enhance the mechanical strength. We find that acrylation of F127 has no significant effect on the formation of micelles, the sol-gel transition temperature, or the lattice structure of concentrated gels. Moreover, the thermal response of the structure for the solutions with compositions below the gel transition are unaffected by crosslinking. However, the viscoelasticity of these solutions is highly enhanced without detriment to their ionic conductivity. In the case of the solutions with compositions near the sol-gel transition, crosslinking produces soft elastomers with outstanding tensile response, whose structure and shear modulus respond reversibly to temperature changes. Our results provide a platform for the design of materials with enhanced viscoelasticity or with elastomeric properties to be used in electrolyte applications. The main advantage of the synthetic strategies proposed here is the use of inexpensive, commercially available copolymers along with the ease in all the synthetic steps.

Acknowledgments

We acknowledge the support of the National Institute of Standards and Technology (NIST), U.S. Department of Commerce, in providing the neutron research facilities used in this work. The statements, findings, conclusions, and recommendations are those of the authors and do not necessarily reflect the views of NIST or the US Department of Commerce. N.J.W. and R.C. acknowledge support of cooperative agreements #70NANB12H239 and 70NANB15H260 from NIST, U.S. Department of Commerce. R.C. acknowledges support from the National Science Foundation Graduate Research Fellowship under Grant No. 1247394. P.J.B acknowledges support from the U.S. Department of Energy, Office of Basic Energy Sciences, Division of Materials Sciences and Engineering under Award No. DE-FG02-09ER46626.

References

1. Torimoto, T.; Tsuda, T.; Okazaki, K.; Kuwabata, S. New Frontiers in Materials Science Opened by Ionic Liquids. *Adv. Mater.* **2010**, *22*, 1196-1221.
2. Welton, T. Room-Temperature Ionic Liquids. Solvents for Synthesis and Catalysis. *Chem. Rev.* **1999**, *99*, 2071-2084.
3. Wilkes, J. S. A short history of ionic liquids-from molten salts to neoteric solvents. *Green Chem.* **2002**, *4*, 73-80.
4. Xu, W.; Angell, C. A. Solvent-Free Electrolytes with Aqueous Solution-Like Conductivities. *Science* **2003**, *302*, 422-425.
5. Armand, M.; Endres, F.; MacFarlane, D. R.; Ohno, H.; Scrosati, B. Ionic-liquid materials for the electrochemical challenges of the future. *Nat. Mater.* **2009**, *8*, 621-629.
6. Seki, S.; Kobayashi, Y.; Miyashiro, H.; Ohno, Y.; Usami, A.; Mita, Y.; Kihira, N.; Watanabe, M.; Terada, N. Lithium Secondary Batteries Using Modified-Imidazolium Room-Temperature Ionic Liquid. *J. Phys. Chem. B* **2006**, *110*, 10228-10230.
7. Zakeeruddin, S. M.; Grätzel, M. Solvent-Free Ionic Liquid Electrolytes for Mesoscopic Dye-Sensitized Solar Cells. *Adv. Funct. Mater.* **2009**, *19*, 2187-2202.
8. Wang, P.; Zakeeruddin, S. M.; Humphry-Baker, R.; Grätzel, M. A Binary Ionic Liquid Electrolyte to Achieve >7% Power Conversion Efficiencies in Dye-Sensitized Solar Cells. *Chem. Mater.* **2004**, *16*, 2694-2696.

9. Lu, W.; Fadeev, A. G.; Qi, B.; Smela, E.; Mattes, B. R.; Ding, J.; Spinks, G. M.; Mazurkiewicz, J.; Zhou, D.; Wallace, G. G.; MacFarlane, D. R.; Forsyth, S. A.; Forsyth, M. Use of Ionic Liquids for p-Conjugated Polymer Electrochemical Devices. *Science* **2002**, *297*, 983-987.
10. Ding, J.; Zhou, D.; Spinks, G.; Wallace, G.; Forsyth, S.; Forsyth, M.; MacFarlane, D. Use of Ionic Liquids as Electrolytes in Electromechanical Actuator Systems Based on Inherently Conducting Polymers. *Chem. Mater.* **2003**, *15*, 2392-2398.
11. Cho, J. ; Lee, J.; He, Y.; Kim, B. ; Lodge, T. ; Frisbie, C. High-Capacitance Ion Gel Gate Dielectrics with Faster Polarization Response Times for Organic Thin Film Transistors. *Adv. Mater.* **2008**, *20*, 686-690.
12. Cho, J. H.; Lee, J.; Xia, Y.; Kim, B.; He, Y.; Renn, M. J.; Lodge, T. P.; Daniel Frisbie, C. Printable ion-gel gate dielectrics for low-voltage polymer thin-film transistors on plastic. *Nat. Mater.* **2008**, *7*, 900-906.
13. Lodge, T. P. A Unique Platform for Materials Design. *Science* **2008**, *321*, 50-51.
14. Noro, A.; Matsushita, Y.; Lodge, T. P. Thermoreversible Supramacromolecular Ion Gels via Hydrogen Bonding. *Macromolecules* **2008**, *41*, 5839-5844.
15. Noro, A.; Matsushita, Y.; Lodge, T. P. Gelation Mechanism of Thermoreversible Supramacromolecular Ion Gels via Hydrogen Bonding. *Macromolecules* **2009**, *42*, 5802-5810.
16. López-Barrón, C. R.; Li, D.; Wagner, N. J.; Caplan, J. L. Triblock Copolymer Self-Assembly in Ionic Liquids: Effect of PEO Block Length on the Self-Assembly of PEO-PPO-PEO in Ethylammonium Nitrate. *Macromolecules* **2014**, *47*, 7484-7495.

17. He, Y.; Lodge, T. P. A thermoreversible ion gel by triblock copolymer self-assembly in an ionic liquid. *Chem. Commun.* **2007**, 2732-2734.
18. He, Y.; Boswell, P. G.; Bühlmann, P.; Lodge, T. P. Ion Gels by Self-Assembly of a Triblock Copolymer in an Ionic Liquids. *J. Phys. Chem. B* **2007**, *111*, 4645-4652.
19. He, Y.; Lodge, T. P. Thermoreversible Ion Gels with Tunable Melting Temperatures from Triblock and Pentablock Copolymers. *Macromolecules* **2008**, *41*, 167-174.
20. Miranda, D. F.; Russell, T. P.; Watkins, J. J. Ordering in Mixtures of a Triblock Copolymer with a Room Temperature Ionic Liquid. *Macromolecules* **2010**, *43*, 10528-10535.
21. Tang, B.; White, S. P.; Frisbie, C. D.; Lodge, T. P. Synergistic Increase in Ionic Conductivity and Modulus of Triblock Copolymer Ion Gels. *Macromolecules* **2015**, *48*, 4942-4950.
22. Susan, M. A. B. H.; Kaneko, T.; Noda, A.; Watanabe, M. Ion Gels Prepared by in Situ Radical Polymerization of Vinyl Monomers in an Ionic Liquid and Their Characterization as Polymer Electrolytes. *J. Am. Chem. Soc.* **2005**, *127*, 4976-4983.
23. Seki, S.; Susan, M. A. B. H.; Kaneko, T.; Tokuda, H.; Noda, A.; Watanabe, M. Distinct Difference in Ionic Transport Behavior in Polymer Electrolytes Depending on the Matrix Polymers and Incorporated Salts. *J. Phys. Chem. B* **2005**, *109*, 3886-3892.
24. Jana, S.; Parthiban, A.; Chai, C. L. L. Transparent, flexible and highly conductive ion gels from ionic liquid compatible cyclic carbonate network. *Chem. Commun.* **2010**, *46*, 1488-1490.
25. Klingshirn, M. A.; Spear, S. K.; Subramanian, R.; Holbrey, J. D.; Huddleston, J. G.; Rogers, R. D. Gelation of Ionic Liquids Using a Cross-Linked Poly(Ethylene Glycol) Gel Matrix. *Chem. Mater.* **2004**, *16*, 3091-3097.

26. Néouze, M.; Bideau, J. L.; Gaveau, P.; Bellayer, S.; Vioux, A. Ionogels, New Materials Arising from the Confinement of Ionic Liquids within Silica-Derived Networks. *Chem. Mater.* **2006**, *18*, 3931-3936.
27. Matsumoto, K.; Endo, T. Confinement of Ionic Liquid by Networked Polymers Based on Multifunctional Epoxy Resins. *Macromolecules* **2008**, *41*, 6981-6986.
28. Matsumoto, K.; Endo, T. Synthesis of Ion Conductive Networked Polymers Based on an Ionic Liquid Epoxide Having a Quaternary Ammonium Salt Structure. *Macromolecules* **2009**, *42*, 4580-4584.
29. Gu, Y.; Zhang, S.; Martinetti, L.; Lee, K. H.; McIntosh, L. D.; Frisbie, C. D.; Lodge, T. P. High Toughness, High Conductivity Ion Gels by Sequential Triblock Copolymer Self-Assembly and Chemical Cross-Linking. *J. Am. Chem. Soc.* **2013**, *135*, 9652-9655.
30. Miranda, D. F.; Versek, C.; Tuominen, M. T.; Russell, T. P.; Watkins, J. J. Cross-Linked Block Copolymer/Ionic Liquid Self-Assembled Blends for Polymer Gel Electrolytes with High Ionic Conductivity and Mechanical Strength. *Macromolecules* **2013**, *46*, 9313-9323.
31. McIntosh, L. D.; Kubo, T.; Lodge, T. P. Morphology, Modulus, and Conductivity of a Triblock Terpolymer/Ionic Liquid Electrolyte Membrane. *Macromolecules* **2014**, *47*, 1090-1098.
32. Cellesi, F.; Tirelli, N.; Hubbell, J. A. Materials for cell encapsulation via a new tandem approach combining reverse thermal gelation and covalent crosslinking. *Macromol. Chem. Phys.* **2002**, *203*, 1466-1472.
33. Sentmanat, M. L. Miniature universal testing platform: from extensional melt rheology to solid-state deformation behavior. *Rheol. Acta* **2004**, *43*, 657-669.
34. Kline, S. R. Reduction and analysis of SANS and USANS data using IGOR Pro. *J. Appl. Cryst.* **2006**, *39*, 895-900.

35. Guinier, A.; Fournet, G. *Small-angle scattering of X-rays*; Wiley: New York, 1955; , pp 268.
36. Matsuoka, H.; Tanaka, H.; Hashimoto, T.; Ise, N. Elastic scattering from cubic lattice systems with paracrystalline distortion. *Phys. Rev. B* **1987**, *36*, 1754-1765.
37. Matsuoka, H.; Tanaka, H.; Iizuka, N.; Hashimoto, T.; Ise, N. Elastic scattering from cubic lattice systems with paracrystalline distortion. II. *Phys. Rev. B* **1990**, *41*, 3854-3856.
38. Beltramo, P. J.; Furst, E. M. Dielectric spectroscopy of bidisperse colloidal suspensions. *J. Colloid Interface Sci.* **2012**, *380*, 34-41.
39. Hammouda, B.; Ho, D.; Kline, S. SANS from Poly(ethylene oxide)/Water Systems. *Macromolecules* **2002**, *35*, 8578-8585.
40. Hammouda, B.; Ho, D. L.; Kline, S. Insight into Clustering in Poly(ethylene oxide) Solutions. *Macromolecules* **2004**, *37*, 6932-6937.
41. Clover, B.; Hammouda, B. SANS from P85/Water-d under Pressure. *Langmuir* **2010**, *26*, 6625-6629.
42. Goldmints, I.; von Gottberg, F. K.; Smith, K. A.; Hatton, T. A. Small-Angle Neutron Scattering Study of PEO $\hat{\wedge}$ PPO $\hat{\wedge}$ PEO Micelle Structure in the Unimer-to-Micelle Transition Region. *Langmuir* **1997**, *13*, 3659-3664.
43. Goldmints, I.; Yu, G.; Booth, C.; Smith, K. A.; Hatton, T. A. Structure of (Deuterated PEO) $\hat{\wedge}$ (PPO) $\hat{\wedge}$ (Deuterated PEO) Block Copolymer Micelles As Determined by Small Angle Neutron Scattering. *Langmuir* **1999**, *15*, 1651-1656.
44. Hvidt, S.; Joergensen, E. B.; Brown, W.; Schillen, K. Micellization and Gelation of Aqueous Solutions of a Triblock Copolymer Studied by Rheological Techniques and Scanning Calorimetry. *J. Phys. Chem.* **1994**, *98*, 12320-12328.

45. Hahn, H.; Eitouni, H. B.; Balsara, N. P.; Pople, J. A. Responsive Solids from Cross-Linked Block Copolymers. *Phys. Rev. Lett.* **2003**, *90*, 155505.
46. Kříž, J.; Dybal, J. Cooperative Preassociation Stages of PEO-PPO-PEO Triblock Copolymers: NMR and Theoretical Study. *J. Phys. Chem. B* **2010**, *114*, 3140-3151.
47. Eisenberg, D.; Kauzmann, W. *The structure and properties of water*; Clarendon P.: Oxford, 1969; .
48. Modig, K.; Pfrommer, B. G.; Halle, B. Temperature-Dependent Hydrogen-Bond Geometry in Liquid Water. *Phys. Rev. Lett.* **2003**, *90*, 075502.
49. López-Barrón, C. R.; Basavaraj, M. G.; DeRita, L.; Wagner, N. J. Sponge-to-Lamellar Transition in a Double-Tail Cationic Surfactant/Protic Ionic Liquid System: Structural and Rheological Analysis. *J. Phys. Chem. B* **2012**, *116*, 813-822.
50. López-Barrón, C. R.; Wagner, N. J. Structural Transitions of CTAB Micelles in a Protic Ionic Liquid. *Langmuir* **2012**, *28*, 12722-12730.

Table of Contents Graphic

Self-assembly of Pluronic F127-diacrylate in ethylammonium nitrate: structure, rheology and ionic conductivity before and after photo-crosslinking

Carlos R. López-Barrón, Ru Chen, Norman J. Wagner, Peter Beltramo

